

## Measurement of $T_{20}(90^\circ)$ in the ${}^1\text{H}(\vec{d}, \gamma){}^3\text{He}$ reaction below deuteron breakup threshold

K. P. Browne and W. K. Pitts

*University of Louisville, Physics Department, Louisville, Kentucky 40292*

M. K. Smith, J. E. McAninch,\* and L. D. Knutson

*University of Wisconsin, Physics Department, Madison, Wisconsin 53706*

(Received 10 November 1995)

The tensor analyzing powers of the  ${}^1\text{H}(\vec{d}, \gamma){}^3\text{He}$  reaction are sensitive to the tensor component of the nucleon-nucleon force, which mixes the  $L=2$   $D$  state into the  ${}^3\text{He}$  ground state wave function. Modern Faddeev calculations of this reaction allow a quantitative comparison to the parametrization of the tensor force in the trinucleon system. The  $T_{20}$  analyzing power was measured at an incident beam energy of 5.25 MeV and a laboratory angle of  $90^\circ$  ( $\theta_{\text{c.m.}} = 92.9^\circ$ ), where the comparison to theory is especially rigorous. The measured value of  $T_{20}(90^\circ_{\text{lab}})$  is  $-0.035 \pm 0.004$ , which differs by  $\approx 3\sigma$  from a recent Faddeev calculation which uses the separable expansion of the Paris potential. [S0556-2813(96)01108-9]

PACS number(s): 21.45.+v, 21.30.Fe, 24.70.+s, 25.10.+s

The  ${}^3\text{He}$  nucleus is one of the few nuclei where both the ground state and continuum wave functions can be exactly calculated, and this is accomplished in the Faddeev formalism. All components of the wave function can be unambiguously calculated with a given free nucleon-nucleon ( $NN$ ) potential, including the small  $L=2$   $D$  state. This wave function component is mixed into the ground state of  ${}^3\text{He}$  by the tensor force. While the percentage  $D$  state is not itself an observable, its value does serve as a useful parametrization of the tensor force in Faddeev calculations. Determination of tensor force effects relies upon the measurement of polarization observables, with the tensor analyzing powers being naturally sensitive to the tensor force acting in the trinucleon system [1]. Precise measurements of the tensor analyzing power of the  ${}^1\text{H}(\vec{d}, \gamma){}^3\text{He}$  reaction, in particular, may be used to parametrize the tensor force through a comparison to new Faddeev calculations of the analyzing powers [2,3]. Since this reaction proceeds through the well-known electromagnetic force, the interaction Hamiltonian is completely described by an expansion of electric and magnetic multipole transitions.

In detail, the tensor analyzing powers are generated through the interference of a channel spin  $S=3/2$  amplitude with either a channel spin  $S=3/2$  or  $S=1/2$  amplitude. For the  ${}^1\text{H}(\vec{d}, \gamma){}^3\text{He}$  reaction, this results in the spin-independent electric transitions giving a tensor analyzing power which is identically zero in the absence of a tensor force [1]. At low energy, the reaction is dominated by the spin-independent  $E1$  transition, which peaks at  $90^\circ$ . In addition, the tensor analyzing power  $T_{20}(90^\circ)$  is also sensitive only to an interference between multipoles of the same polarity, i.e., the ( $E1$ - $E1$ ), ( $M1$ - $M1$ ), ( $E2$ - $E2$ ), and ( $M1$ - $E2$ ) interferences. The reaction matrix elements have been measured at  $E_d=10$  MeV, with the  $M1$ ,  $E2$ , and spin-flip  $E1$  contributions found to be much smaller than the spin-independent

$E1$  transitions [4]. In short, a measurement of  $T_{20}(90^\circ)$  at low energy should be almost exclusively dominated by contributions of the tensor force, manifest through  $E1(S=3/2)$ - $E1(S=1/2)$  interference.

We report here a measurement of the tensor analyzing power  $T_{20}(90^\circ_{\text{lab}})$  ( $92.9^\circ$  in the c.m. system). The beam energy was chosen to be below the deuteron breakup threshold of 6.6 MeV, closing the breakup reaction channel. This new measurement utilized the same basic techniques and equipment as the earlier experiments of Goeckner *et al.* [4,5]. A polarized deuteron beam was produced in an atomic beam source with subsequent ionization of the  $\text{D}^0$  atoms in a cesium beam [6]. A Wein filter oriented the beam to produce a pure  $t_{20}$  beam at the target. The polarimeter was based upon the  ${}^3\text{He}(\vec{d}, p){}^4\text{He}$  reaction and calibrated to the absolute polarization standard of the  ${}^{16}\text{O}(\vec{d}, \alpha_3){}^{14}\text{N}$  reaction [7,8]. The scale uncertainty of the polarimeter is less than 2% of the measured average value of  $t_{20}=0.635$ .

The beam was bunched at a frequency of 5.2 MHz and accelerated to 6.70 MeV. The target cell was 14 cm long, with a viewed region of  $\pm 3.0$  cm about the midpoint of the cell, with the beam energy being 5.25 (+0.55, -0.63) MeV about the midpoint. The deuteron beam energy was always below the breakup energy of 6.6 MeV throughout the gas volume. Reaction photons were detected in a large (25 cm  $\times$  25 cm) NaI spectrometer with an active shield [9]. Photons from the  ${}^1\text{H}(\vec{d}, \gamma){}^3\text{He}$  reaction ranged in energy from 7.01 to 7.41 MeV. The background under the  ${}^1\text{H}(\vec{d}, \gamma){}^3\text{He}$  capture peak included photons from thermal neutron capture in the spectrometer as well as photons from the interaction of the primary deuteron beam with the cell and beam line components. The background was reduced by placing lead or tantalum shields in front of all low- $Z$  materials (e.g., epoxy adhesives or aluminum) exposed to a scattered beam. Tungsten shadow bars were placed on the direct line of sight from the entrance and exit foils to the sodium iodide spectrometer. Both lead and wax shielding was placed on the direct line of sight from the spectrometer to slits in the beam line. The exit

\*Present address: L-397, Lawrence Livermore National Laboratory, Livermore, California.

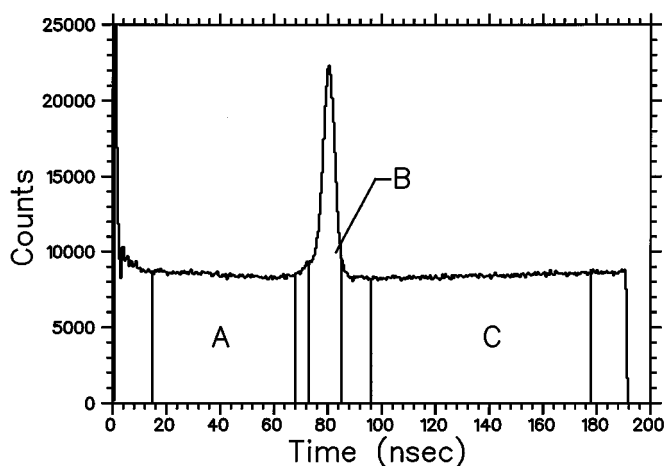


FIG. 1. Time of flight spectrum from the NaI spectrometer, illustrating the TOF sorting conditions. Region *B* is the true TOF region, while regions *A* and *C* are the low TOF and high TOF regions, respectively.

beam line and inner wall of the target chamber were lined with lead and tantalum, respectively.

The target cell was filled with 99.999% pure hydrogen gas at 2550 mbar and 90 K. A major consideration in the design of the gas handling system was the need to eliminate nitrogen in the target gas. The stripping reactions  ${}^{14}\text{N}(\vec{d}, p){}^{15}\text{N}^*$  and  ${}^{14}\text{N}(\vec{d}, n){}^{15}\text{O}^*$  have large cross sections for the production of high energy photons. Metal and ceramic components were used in the gas handling system wherever possible, with most components being routinely baked to 200 °C while under clean vacuum. The only organic components wetted by the target gas were one O ring and the epoxy adhesive at the entrance and exit foils. The cell was filled through a molecular sieve cold trap cooled to 77 K. A second cold trap, also at 77 K, was open to the cell after filling.

A typical time of flight spectrum is shown in Fig. 1. The large central peak is due to photons produced during the passage of the beam bunch through the cell. Particles with a longer flight time (e.g., fast neutrons) would appear to the left of this peak. The flatness of the background around the central peak shows that the neutron background was due to thermal neutron capture in the NaI detector. Flight times of thermal neutrons are effectively random on the time scale of the 192 ns period of the bunched beam. This background was removed by subtracting a normalized sample of the flat background from the events with the proper time of flight. The three timing gates used to sort events by time of flight are shown in Fig. 1. The defined sorting gate for photons of interest is the true TOF gate are shown in Fig. 1. The low TOF and high TOF timing gates are used to produce pulse height spectra which result from thermal neutron capture. A pulse height spectrum, with photon sorting conditions, was prepared by subtracting the thermal neutron background (i.e., either the low TOF or high TOF gated pulse height spectrum, properly normalized from the ratio of gate width to the true TOF gate width) from the true TOF pulse height spectrum. Either gated spectrum gave the same final asymmetry, and an average of the low and high TOF gated spectra was used in the final analysis.

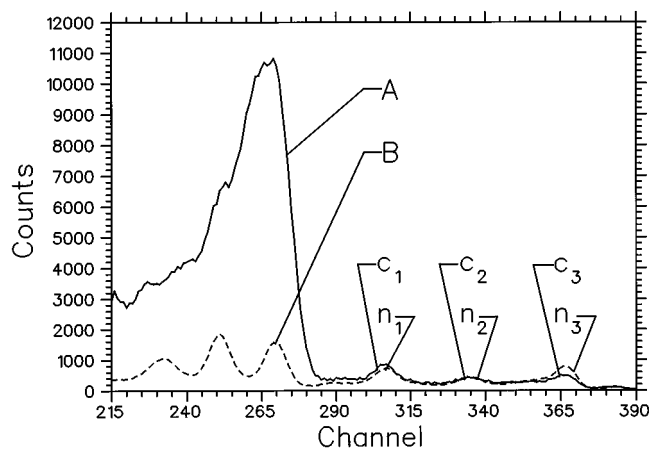


FIG. 2. Pulse height spectra from the NaI spectrometer, showing the effect of nitrogen contamination. The solid line (*A*) results from a hydrogen-filled target, with the random neutron background subtracted. The dashed line (*B*) results from a nitrogen-filled target. The hydrogen spectrum has been normalized to the nitrogen spectrum at peaks *c*<sub>1</sub>, *c*<sub>2</sub>, and *c*<sub>3</sub>.

The most significant source of background in the random neutron subtracted photon spectrum resulted from the photon decay of excited states in  ${}^{15}\text{N}$  and  ${}^{15}\text{O}$ . Because the cross sections for these reactions with nitrogen are much larger than the  ${}^1\text{H}(\vec{d}, \gamma){}^3\text{He}$  cross section, even a small amount of nitrogen in the hydrogen gas generates a large background of high energy photons with flight times in the true TOF sorting window. There was a small residual nitrogen contamination, shown by the presence of the three small peaks (labeled *c*<sub>1</sub>, *c*<sub>2</sub>, and *c*<sub>3</sub>) above the  ${}^1\text{H}(\vec{d}, \gamma){}^3\text{He}$  capture peak in Fig. 2. These peaks were also present when the cell was filled with nitrogen (labeled *n*<sub>1</sub>, *n*<sub>2</sub>, and *n*<sub>3</sub> in Fig. 2). The true TOF pulse height spectrum from the nitrogen target is used for the subtraction of the contaminant, after normalizing and aligning the three marker peaks in the nitrogen spectrum

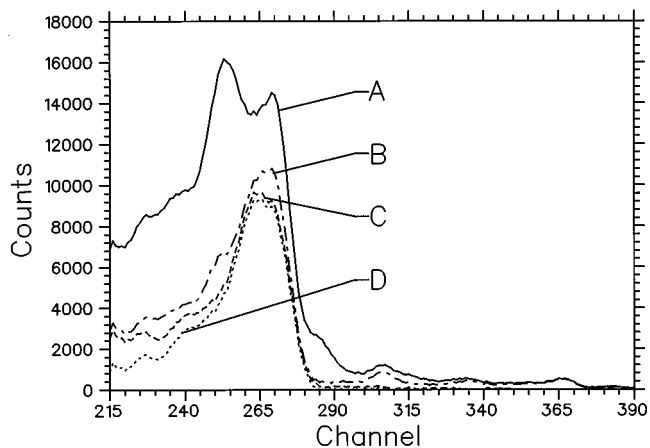


FIG. 3. Pulse height spectra from the NaI spectrometer, showing the subtracted backgrounds. The dashed line (*A*) is the raw data, while the long-dashed line (*B*) shows the same spectrum after subtraction of the random neutron background. The short-dashed line (*C*) shows spectrum *B* after subtraction of the nitrogen contamination. The dotted line (*D*) is spectrum *C* after subtraction of the exponential background under the radiative capture peak.

TABLE I. Estimates of the uncertainty.

Contribution	Uncertainty
Statistical error	$\pm 0.0037$
$N_2$ subtraction (statistical)	$\pm 0.0018$
$N_2$ subtraction (systematic)	$\pm 0.0007$
Background (magnitude)	$\pm 0.0003$
Background (asymmetry)	$\pm 0.0003$
Dead time	$\pm 0.00002$
Errors added in quadrature	$\pm 0.0042$

with the same three peaks in the  ${}^1\text{H}(\vec{d}, \gamma){}^3\text{He}$  spectrum. Peak sums for  $n_1$ ,  $n_2$ , and  $n_3$  were extracted from the nitrogen spectra, and a separate normalization determined from each peak sum. Each of these normalized, spin-sorted nitrogen spectra was then subtracted from the corresponding spin-sorted  ${}^1\text{H}(\vec{d}, \gamma){}^3\text{He}$  capture spectrum, and propagated independently through the analysis. The quoted systematic error of the nitrogen subtraction was generated from the spread of the final  $T_{20}$  values with these different normalizations. The final spectrum which resulted from the subtraction of both the random neutron background and the average nitrogen contribution is shown in Fig. 3. A plot of the unsubtracted pulse height spectrum, corresponding to the true TOF gate, is shown for comparison. An additional background in the random neutron subtracted spectra was due to the entrance and exit foils. The only significant photon peak was at about 3.7 MeV energy, superimposed on an exponential background. The energy of this peak was consistent with a doublet in  ${}^{13}\text{C}$ , presumably formed by deuteron stripping reactions upon pump oil deposits frozen onto the foils of the target.

The final spectrum is shown as curve *D* in Fig. 3. Curve *A* in Fig. 3 is the true TOF gated spectrum, curve *B* is the same spectrum after subtraction of the random neutron background, and curve *C* results from the nitrogen subtraction applied to curve *B*. Final peak sums were taken between channels 254 and 284 in this spectrum, minus a fitted exponential background. The functional form for the fit was modeled after that used in other capture experiments at Wisconsin [10]. It included a constant background, a Gaussian main peak, a Gaussian first escape peak, a Gaussian second escape peak, a high energy exponential tail on the main peak, a low energy exponential tail on the main peak, and an exponential background. This fitted exponential background includes the background due to beam interaction with the target cell, in the energy region of interest. Measurements with an empty cell showed that the “true” gated energy spectrum from the empty cell consisted only of an exponential background with no statistically significant analyzing power. The exponential component of the fit to the final spectrum then automatically includes the background due to the cell. This procedure was chosen as an alternative to direct subtraction of empty target spectra. When the target cell was empty, the beam energy at the exit foil was significantly higher, giving more background from the exit foil, than when the target was

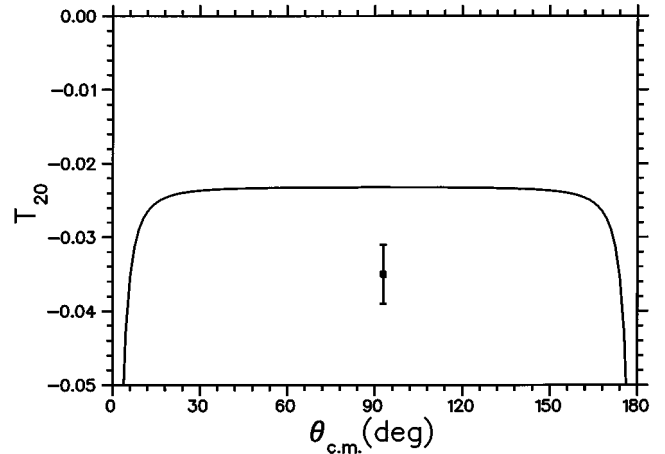


FIG. 4. Comparison of the datum point to a modern Faddeev calculation of the  ${}^1\text{H}(\vec{d}, \gamma){}^3\text{He}$  calculation. The calculation is that of Fonseca and Lehman, at an incident energy of 5.25 MeV. The  $NN$  potential is the separable expansion of the Paris potential. The  $NN$   $P$  waves are included.

full. The uncertainty of the fitted background was determined by making a series of fits and defining the uncertainty to be the extreme spread of solutions with similar  $\chi^2$  values. The average value of the exponential background was used to calculate  $T_{20}$  from these data.

The final value of  $T_{20}$  from this measurement is  $T_{20} = -0.035 \pm 0.004$ , including both the estimated statistical and systematic uncertainties. All contributions to the uncertainty are listed in Table I. Not included is the scale uncertainty of 2% due to the polarimeter calibration.

The measured value for  $T_{20}(90^\circ)$  is compared in Fig. 4 to the theoretical calculation of Fonseca and Lehman [3]. This calculation includes a full three-body wave function in both the ground state and the continuum. The continuum  $P$  waves are included, and their effect has been shown to be essential in reproducing  $T_{20}(\theta)$  at these energies. The potential is the separable expansion of the Paris potential (PEST). Only the  $E1$  multipole is included at this time. It seems likely that the  $E1$ - $E1$  interference terms should dominate  $T_{20}(90^\circ_{\text{lab}})$  at this energy, demonstrated in a matrix element fit by Goeckner at  $E_d = 10$  MeV [4]. Note that the disagreement between the experiment and the calculation is nearly  $3\sigma$ . The disagreement may be due to the parametrization of the tensor force in the PEST, some problem with the present description continuum  $P$  waves, or possibly the lack of the  $E2$  and  $M1$  multipoles in the present calculations. Additional theoretical work will be required to answer this question.

We would like to thank Professor A.C. Fonseca and Professor D.R. Lehman for their calculation of  $T_{20}(\theta)$  which we quoted here. We would also like to acknowledge the assistance of Thomas Finessey in carrying out this measurement, and the support provided by the University of Louisville Graduate Research Council. The work of the Wisconsin group is supported by the National Science Foundation under Contract No. PHY-9316221.

- [1] H.R. Weller and D.R. Lehman, *Annu. Rev. Part. Nuc. Sci.* **38**, 563 (1988).
- [2] S. Ishikawa and T. Sasakawa, *Phys. Rev. C* **45**, R1428 (1994).
- [3] A.C. Fonseca and D.R. Lehman, *Phys. Rev. C* **48**, R503 (1993).
- [4] F. Goeckner, W.K. Pitts, and L.D. Knutson, *Phys. Rev. C* **45**, 2536 (1992).
- [5] F.C. Goeckner, Ph.D. thesis, University of Wisconsin, 1991, available from University Microfilms, Ann Arbor, MI 48106.
- [6] W. Haeberli, M.D. Barker, C.A. Gossett, D.G. Mavis, P.A. Quin, J. Sowinski, T. Wise, and H.F. Glavish, *Nucl. Instrum. Methods* **196**, 319 (1982).
- [7] K. Stephenson and W. Haeberli, *Nucl. Instrum. Methods* **169**, 483 (1980).
- [8] N. Rodning, Ph.D. thesis, University of Wisconsin, 1984, available from University Microfilms, Ann Arbor, MI 48106.
- [9] C. Gosset, Ph.D. thesis, University of Wisconsin, 1983, available from University Microfilms, Ann Arbor, MI 48106.
- [10] T.R. Wang *et al.*, *Phys. Rev. C* **37**, 2301 (1988).